J Appl Electrochem (2011) 41:925–937
DOI 10.1007/s10800-011-0318-8

ORIGINAL PAPER

Preparation and characterisation of carbon-supported palladium nanoparticles for oxygen reduction in low temperature PEM fuel cells

G. F. Alvarez · M. Mamlouk · S. M. Senthil Kumar · K. Scott

Received: 16 December 2010 / Accepted: 18 April 2011 / Published online: 30 April 2011

Abstract Pd nanoparticles have been synthesised using different reducing agents, including ethylene glycol (EG), formaldehyde and sodium borohydride and their activity for the oxygen reduction reaction (ORR) evaluated. The use of EG led to the best morphology for the ORR and this synthetic method was optimised by adjusting the system pH. Carbon-supported Pd nanoparticles of approximately 7 nm diameter were obtained when reduction took place in the alkaline region. Pd synthesised by EG reduction at pH 11 presented the highest mass activity 20 A g^{-2} and active surface area 15 m^2 g^{-1}. These synthetic conditions were used in further synthesis. The effect of heat treatment in H_2 atmosphere was also studied; and increased size of the palladium nanoparticles was observed in every case. The Pd/C catalyst synthesised by reduction with EG at pH 11 was tested in a low temperature H_2/O_2 (air) PEMFC with a Nafion® 112 membrane, at 20 and 40 °C. Current densities at 0.5 V, with O_2 fed to the cathode, at 40 °C were 1.40 A cm^{-2} and peak power densities 0.79 W cm^{-2}, approximately; which compared with 1.74 A cm^{-2} and 0.91 W cm^{-2}, respectively for a commercial Pt/C.

Keywords Pd nanoparticles · Ethylene glycol synthesis · Oxygen reduction reaction · Polymer electrolyte membrane fuel cells

G. F. Alvarez · M. Mamlouk (✉) · S. M. Senthil Kumar · K. Scott
School of Chemical Engineering and Advanced Materials, Newcastle University, Newcastle Upon Tyne NE1 7RU, UK
e-mail: mohamed.mamlouk@ncl.ac.uk

1 Introduction

Polymer electrolyte membrane (PEM) fuel cells have been considered as a good alternative to internal combustion engines because of their high power density, high energy conversion efficiency and low emission level. Their technology is currently well developed, however it suffers from several limitations. These limitations include low value of waste heat, which decreases the overall efficiency, difficult water balance, to avoid both flood and dryness, and difficult heat balance to maintain the operating temperature. Another important issue of current PEM fuel cells is their cost. They are usually platinum catalyzed and the price of the platinum catalyst contributes to make these fuel cells expensive. For instance, for automotive applications, the reported platinum consumption was of over 75 g Pt per vehicle [1]. Considering the average price of platinum in the last 5 years, nearly 1,200 US$ per troy ounce, according to Johnson Matthey prices, the cost of only the platinum will raise to around 3,000 US$ per car. This is a clear indicator or the immediate need of finding an alternative material to platinum to catalyze PEM fuel cells.

Many efforts have been done in this field; some of them involved the replacement of some platinum with alternative less expensive metals. This approach has yielded competitive catalysts, like PtNi, PtCo, PtFe or PtIr alloys for the oxygen reduction reaction (ORR), but the cost is still very high [2–6]. Therefore, the most ambitious approach to this problem is to replace platinum with less expensive materials while maintaining an electrocatalytic activity at least equal to that of state-of-the-art Pt catalysts. Palladium based catalysts have been reported as interesting alternatives to catalyze PEM fuel cells [7–10]. Also, considering that the average price of palladium in the last 5 years was nearly one quarter of the price of platinum, approximately

300 US$ per troy ounce, palladium based catalysts appear as promising candidates to replace platinum.

Palladium is a noble metal with high catalytic activity, which is used in some relevant industrial processes, however its use is less extensive than platinum [11]. It is more abundant than platinum in the earth crust and its price is considerably lower. In electrocatalysis, palladium based catalysts have demonstrated to be good in their use for organic fuel oxidation [12] and also being able to store and release substantial amounts of hydrogen [13]. Studies of palladium and palladium alloys catalytic activity for oxygen reduction have been reported since the 1960s [14]. Early preparations of carbon-supported Pd catalyst were reported by Chaston et al. in 1961, they studied the reduction of Pd salts on activated charcoal [15], similar publications followed this one, as for instance the ones from Pope et al. and Bond [16, 17]. Moreira et al. reported in 2004 the preparation of carbon supported palladium catalysts, by an impregnation method and H_2 reduction at 300 °C, Pd/C (on activated carbon) and Pd/Vulcan [18] and concluded that performance for Pd/Vulcan was better than for Pd/C.

This study aim was to identify suitable preparation conditions for Pd nano-particles for their use as an alternative to platinum as a catalyst for ORR in PEM fuel cells. Prepared metal nanoparticles were supported on carbon black, Vulcan XC-72R. Initial tests were carried out in a half cell and successful candidates were tested as cathode materials in a low temperature PEM fuel cell. The preparation method was by impregnation followed by reaction with a reducing agent which has been a popular method for catalyst preparation [18–21].

2 Experimental

Electrocatalysts were prepared by reduction of the palladium precursor, ammonium tetrachloropalladate (II) (Aldrich, 99.995% trace metals basis), using different reducing agents; ethylene glycol (Aldrich, ≥99%), formaldehyde and sodium borohydride. Reductions with EG, using the polyol method [22], was carried out under N_2 flow to minimise the number of oxidised species in the catalysts [23]. Synthesis with the other two reducing agents was carried out under air. Further catalyst preparations were carried out using the polyol method and maintaining an alkaline pH, in order to optimise the synthesis method. pH was adjusted by adding drops of prepared 0.1 M NaOH (Alfa Aesar 97%) solution. The carbon support used was Vulcan XC-72R (Cabot), which was pre-treated refluxing the carbon for 16 h at 120 °C in a solution containing 7 mol dm^{-3} (M) of HNO_3 [24]. Prior to metal deposition, pre-treated carbon was thoroughly washed with deionised water until the pH was close to neutral. The studied catalysts were given the following symbols:

Pd/C-Etek Pd catalyst purchased from E-Tek.
Pd/C–EG Reduction with ethylene glycol.
Pd/C–EG-300 reduction with ethylene glycol and treatment in H_2 at 300 °C.
Pd/C–CH_2O reduction with formaldehyde.
Pd/C–CH_2O-300 reduction with formaldehyde and treatment in H_2 at 300 °C.
Pd/C–$NaBH_4$ reduction with sodium borohydride.
Pd/C–$NaBH_4$-300 reduction with sodium borohydride and treatment in H_2 at 300 °C.
Pd/C–EG10 reduction with ethylene glycol at pH 10.
Pd/C–EG11 reduction with ethylene glycol at pH 11.
Pd/C–EG12 reduction with ethylene glycol at pH 12.
Pd/C–EG13 reduction with ethylene glycol at pH 13.
Pd/C–EG11-untr reduction with ethylene glycol at pH 11 on as-received Vulcan XC-72R.

Electrochemical characterisations were initially carried out using a three-electrode cell. As a working electrode was used a rotating disc electrode (RDE), EDI101 from Radiometer Analytical, and electrochemical data was collected with a BAS Epsilon potentiostat. The electrolyte used in the electrochemical cell was 0.5 mol dm^{-3} H_2SO_4 at room temperature. The RDE tip was glassy carbon with 3 mm diameter and the metal loading used was 86 μg cm^{-2}. The reference electrode was a silver chloride saturated KCl electrode, +0.197 V versus NHE, and the counter electrode was a coiled platinum wire, 23 cm long and 0.5 mm diameter. Before each electrochemical test for all Pd/C catalysts an electrode conditioning was performed by using cyclic voltammetry (CV) method. The initial potential was the open circuit potential, ca. 0.8 V, and scans were performed between 1.24 and 0.07 V versus NHE; final potential was 1.24 V with a scan rate of 50 mV s^{-1} about 10 cycles in nitrogen saturated 0.5 M H_2SO_4 solution. In contrast with platinum, it was difficult to determine the charge of a monolayer of adsorbed hydrogen on a Pd catalyst due to the ability of bulk palladium to absorb hydrogen [25, 26]. Therefore, quantification of the electrochemical surface area (ECSA) was obtained from the oxide reduction peak based on the fact that the charge of a monolayer of adsorbed oxygen for a smooth palladium electrode is twice as large as hydrogen monolayer, $Q_H = ½Q_O$ ($Q_H = 210$ μC cm^{-2}) [26–28]. The ECSA was calculated from the charge of the monolayer of chemisorbed oxygen and corrected for the metal loading employed for electrode fabrication.

Membrane electrode assemblies (MEAs) were prepared with metal loadings of 0.2 mg cm^{-2} of Pt in the anode and 0.6 mg cm^{-2} of metal in the cathode. Nafion® 112 was used as electrolyte membrane. Pt/C purchased from Etek

was used as anode material in each case. The catalyst layer was sprayed on a commercial gas diffusion layer, a low temperature microporous layer (GDL LT 1200-W, Etek). The cell body was made of graphite with 1 cm × 1 cm parallel flow fields. The temperature of the cell was controlled by cartridge heaters inserted into the cell body. Operation temperatures were 20 °C, or room temperature, and 40 °C. H_2 was used as a fuel and either air or oxygen was used as an oxidant. Gases were fed at atmospheric pressure.

3 Results and discussion

3.1 Physicochemical characterization

Catalysts loadings estimated from EDX analysis are shown in Table 1. Accordingly to the preparation procedure, complete deposition of Pd precursor on the carbon would lead to a 20% weight palladium catalysts. Deviations from the nominal value may be due to either carbon loss during the washing process or an incomplete Pd deposition on the carbon surface.

Catalysts were examined by transmission electron microscopy (TEM). As an example the TEM images of Pd/C–EG, Pd/C–CH_2O and Pd/C–$NaBH_4$ are shown in Fig. 1. While in general all prepared palladium catalysts exhibited agglomeration of metal nanoparticles, clear distinction can be seen between the morphology of the three prepared catalysts. Pd prepared with CH_2O showed the smallest particles size in comparison to the other two synthesised catalysts, however its catalyst particles' distribution over the carbon support was very poor with most of the particles attached together (agglomerates). Both Pd/C–EG and Pd/C–$NaBH_4$ exhibited good Pd particles distribution over the carbon support with Pd/C–EG exhibiting smaller average particle size (see Table 1). Some individual particles were measured from the TEM pictures and the observed size was around the calculated average value from the X-ray diffraction spectra.

Figure 2a shows XRD patterns corresponding to carbon-supported palladium catalysts initially prepared using three different reducing agents, both before and after treatment in H_2 at 300 °C. All carbon-supported palladium catalysts were characterised by using X-ray diffraction. All samples showed peaks matching those of palladium face-centered cubic (fcc) lattice, diffraction patterns corresponding to palladium oxides were not observed in any case. Peak (220), which was considered not to be influenced by the presence of carbon, was used for calculations. Particle size and Pd–Pd bond distance were calculated from Scherrer and Bragg equations, respectively. The broad peak at a 2θ of approximately 25° in each spectra was due to the carbon support [29]. The average Pd–Pd bond distance, d, was calculated for each carbon-supported palladium catalyst prepared using Bragg equation. The average value was found to be 0.2751 ± 0.0003 nm, in agreement with the ICDD data for palladium (00-046-1043). Particle sizes are shown in Table 1.

The smallest particles were obtained using formaldehyde as the reducing agent. Particle sizes for Pd/C–EG and Pd/C–$NaBH_4$ were similar to each other and much larger than those of Pd/C–CH_2O, as can be seen from a simple comparison of spectra peaks; peaks corresponding to the

Table 1 Particle size, ECSA and metal loading for carbon-supported palladium catalysts

Catalyst	Particle size (nm)	ECSA ($m^2\ g^{-1}$)	Metal load (wt%)
Pd/C–EG	10.7	6.1	21.7
Pd/C–EG-300	21.8	2.0	21.7
Pd/C–CH_2O	5.2	9.6	18.7
Pd/C–CH_2O-300	18.1	3.1	18.7
Pd/C–$NaBH_4$	11.7	4.4	19.1
Pd/C–$NaBH_4$-300	18.8	2.4	19.1
Pd/C–EG10	5.8	11.7	26.5
Pd/C–EG11	5.7	15.4	34.1
Pd/C–EG12	7.7	10.6	29.2
Pd/C–EG13	5.8	15.3	23.3
Pd/C–EG11-untr	7.3	14.6	22.5
Pd/C–EG11-untr-100	11.2	–	–
Pd/C–EG11-untr-200	14.1	–	–
Pd/C–EG11-untr-300	16.5	–	–
Pd/C-Etek	3.5	15.7	19.9
Pt/C-Etek	3.4	55.3	19.8

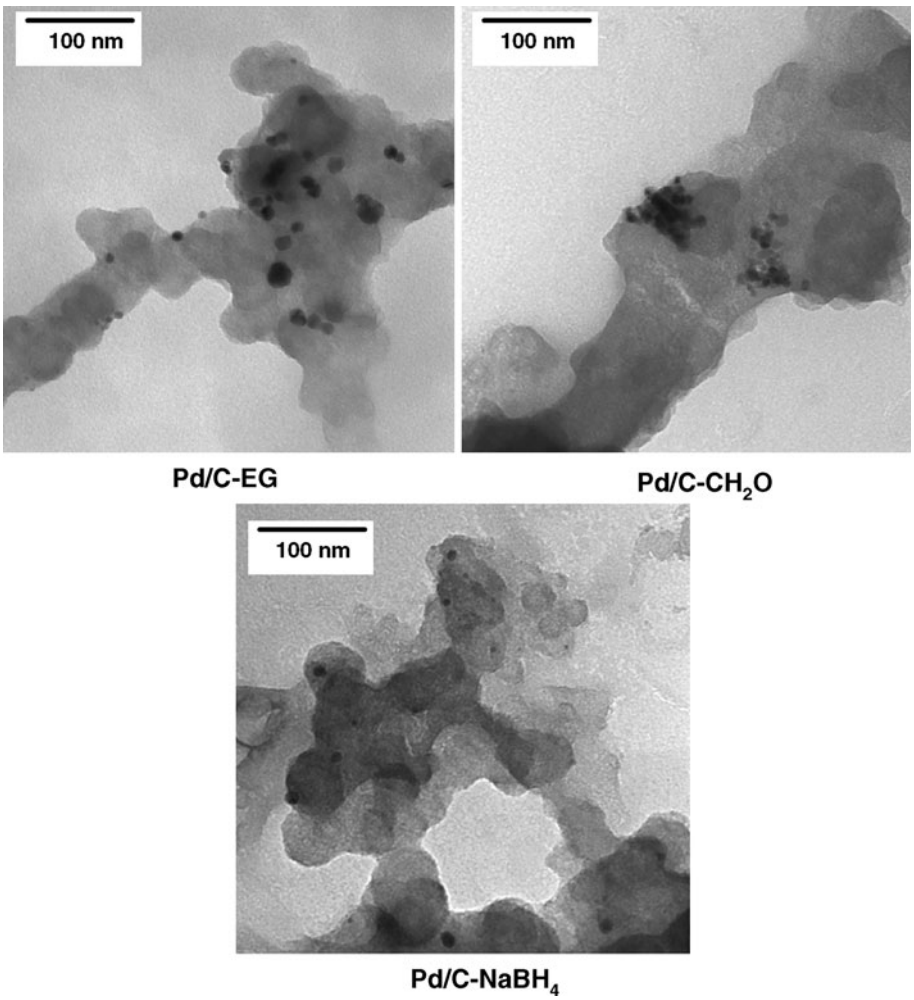

Fig. 1 TEM image of Pd/C–EG, Pd/C–$NaBH_4$ and Pd/C–CH_2O

face-centered cubic lattice of Pd were wider and shorter for Pd/C–CH_2O, which indicates smaller particles. When catalysts were treated at 300 °C under H_2, particle growth was observed in every catalyst. Larger growth was experienced by smaller palladium nanoparticles. Those of Pd/C–CH_2O increased from 5 nm diameter before heat treatment to 18 nm after, particles in Pd/C–EG and Pd/C–$NaBH_4$ increased from 11 and 12 to 22 and 19 nm, respectively. Commercial Pd/C from Etek was also characterized. It had the smallest Pd nanoparticles initially, 3.5 nm, and suffered the biggest sintering, 16 nm after treatment.

Figure 2b shows XRD patterns for catalysts prepared by ethylene glycol reduction with pH control. All carbon-supported palladium nanoparticles prepared by ethylene glycol reduction in basic media were smaller than those prepared without pH control. Thus, it could be concluded that the synthesis of Pd/C was strongly influenced by the pH of the reaction mixture. The reduction of the palladium precursor salt in basic media led to smaller Pd particles and, within the pH range from 10 to 13, no significant differences in size were observed. Pd/C–EG11-untr, prepared by EG reduction at pH 11 on as-received Vulcan XC-72R, also had particle size close to all catalysts prepared on pre-treated carbon in basic conditions.

When catalysts prepared by ethylene glycol reduction with pH control were treated at 300 °C under H_2 they all exhibited particle growth. To study further the effect of temperature on the sintering Pd/C–EG11-untr was treated in H_2 at 100, 200 and 300 °C. XRD spectra of these catalysts are shown on Fig. 2c. Particle sizes increased linearly with temperature. Particle size increased from 6 to 11 nm at 100 °C, to 14 nm at 200 °C and to 17 nm at 300 °C. This particle growth with the temperature has been previously reported in both nitrogen [30] and hydrogen [31] atmosphere.

3.2 Electrochemical characterization

A typical CV of Pd/C deposited on glassy carbon is shown in Fig. 3. The initial potential was the open circuit potential, ca. 0.8 V, and scans were performed between 1.24 and 0.07 V versus NHE; final potential was 1.24 V. On the positive sweep, only current corresponding to the double layer charging current was recorded in the potential range

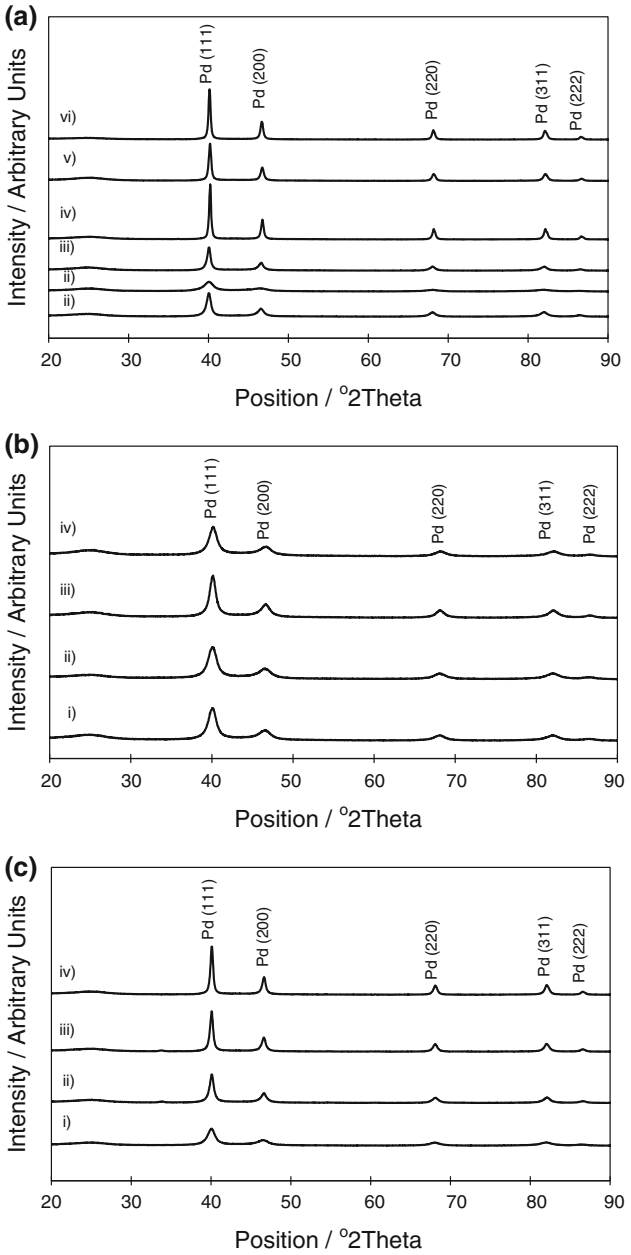

Fig. 2 XRD patterns of carbon-supported palladium catalysts. **a** (i) Pd/C–EG, (ii) Pd/C–CH_2O, (iii) Pd/C–$NaBH_4$, (iv) Pd/C–EG-300, (v) Pd/C–CH_2O-300 and (vi) Pd/C$NaBH_4$-300. **b** (i) Pd/C–EG10, (ii) Pd/C–EG11, (iii) Pd/C–EG12 and (iv) Pd/C–EG13. **c** (i) Pd/C–EG11-untr-rt, (ii) Pd/C–EG11-untr-100, (iii) Pd/C–EG11-untr-200 and (iv) Pd/CEG11-untr-300

from ca. 0.3 to 0.75 V versus NHE. Oxidation of the palladium surface started at ca. 0.75 V and a small peak at ca. 1.04 V was also observed; these results matched previous observations [32, 33]. In the negative potential sweep oxide reduction started at ca. 0.83 V with the peak positions located at ca. 0.72 V. From ca. 0.55 V to 0.3 V only the double layer charging current was observed in the cathodic sweep. When the electrode potential was below

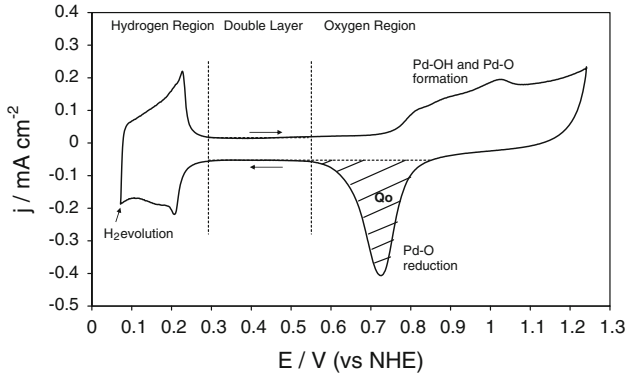

Fig. 3 Cyclic voltammogram of Pd/C–EG11-untr in N_2 saturated 0.5 M H_2SO_4 solution at room temperature, scan rate 5 mV s^{-1}

ca. 0.3 V a cathodic current was recorded. This current was believed to be due, initially, to hydrogen adsorption on the palladium surface and, at lower potentials, also to the dissolution of hydrogen in the bulk of the palladium [26].

Palladium dissolution in sulphuric acid solution was reported to start at potentials close to 0.96 in the anodic sweep [25, 34]. Thus, peaks corresponding to its anodic dissolution could not be discriminated from the oxygen adsorption peaks. After the electrode conditioning, none of the synthesised carbon-supported palladium catalyst presented evidence of dissolution. Nevertheless, dissolution rate would depend on the metal surface area; therefore catalysts with smaller metal particles, which would imply higher surface area per given metal loading, would dissolve faster.

Evidence of dissolution during conditioning was seen for commercial Pd/C, which particle diameter, 3.5 nm, was approximately half of Pd/C–EG11-untr. Figure 4 shows voltammograms corresponding to 80 cycles at scan rate 50 mV s^{-1} of a Pd/C from Etek electrode. A dissolution peak at ca. 0.96 V could not be differentiated; however the loss of electrochemical surface area was dramatic. The decrease of the area under the oxide reduction peak could be appreciated after each cycle. Palladium dissolution during the electrode conditioning, also called electrochemical activation, of palladium nanoparticles in 0.5 M H_2SO_4 was also reported elsewhere [35]. Although Pd/C purchased from Etek did not present a stable voltammogram after electrode conditioning, its slow cyclic voltammogram recorded straight after the conditioning was still used for comparison.

Figure 5a compares cyclic voltammograms of Pd/C–EG, Pd/C–CH_2O and Pd/C–$NaBH_4$ to the Pd/C from Etek. A large difference in the electrochemical surface area (ECSA) was observed between commercial Pd/C and those catalysts prepared without pH control. Commercial Pd/C had ECSA of 16 m^2 g^{-1}; whilst for Pd/C–CH_2O, Pd/C–EG and Pd/C–$NaBH_4$ values were 10, 6 and 4 m^2 g^{-1},

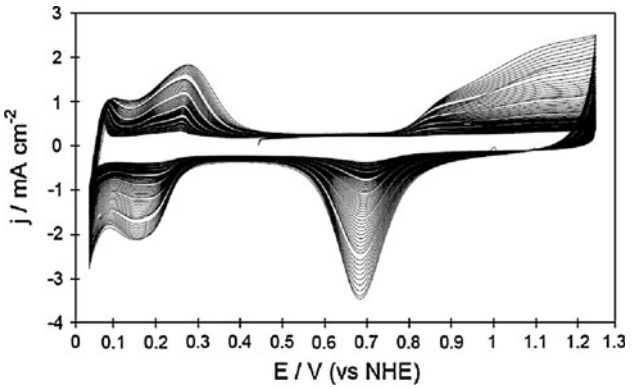

Fig. 4 Cyclic voltammogram of Pd/C from Etek in N_2 saturated 0.5 M H_2SO_4 solution at room temperature, scan rate 50 mV s^{-1}. The plot shows the first 80 potential cycles of the electrode

respectively. Electrochemical surface area measurements were in agreement with palladium particle sizes calculated from the XRD diffractograms, smaller particles lead to higher surface areas (Table 1).

Figure 5a also shows the oxide reduction peak positioned at different potentials for different Pd catalysts. Potential values were approximately 0.70 V for Pd/C-Etek, 0.72 V for Pd/C–CH_2O and 0.74 V for Pd/C–EG and Pd/C–$NaBH_4$ versus NHE. This shift in potentials seemed to be related to size of the palladium particles; catalysts with smaller particles presented oxide reduction peaks at lower potentials. This behaviour has been previously reported for carbon-supported platinum nanoparticles [36]. The Pt oxide reduction peak was reported to shift progressively to negative potentials with decreasing size of platinum particles. This behaviour was believed to be due to stronger adsorption of the OH groups in smaller particles caused by an increase in low coordination sites with the decrease of the particle diameter [37].

Pd/C–CH_2O gave low activity towards ORR (as discussed below) despite having the highest ECSA. Pd/C–$NaBH_4$ presented both low ECSA and low activity for ORR. Pd/C–EG gave an intermediate ECSA value and the highest ORR activity of these three catalysts. Thus, ethylene glycol was chosen as reducing agent for the following syntheses.

The particle size for Pd–EG without monitoring the pH was ca. 11 nm. Pd or palladium alloy particles of size around 5 nm were reported in the literature [29, 38–40]. Therefore, the next step in this study was to find an optimum pH for the ethylene glycol reduction; thus four additional Pd/C catalysts were prepared by ethylene glycol reduction. pH range was restricted to the basic region, with pH values between 10 and 13. Cyclic voltammograms in N_2 saturated 0.5 M $H_2SO_4^-$ for those four catalysts are compared in Fig. 5b.

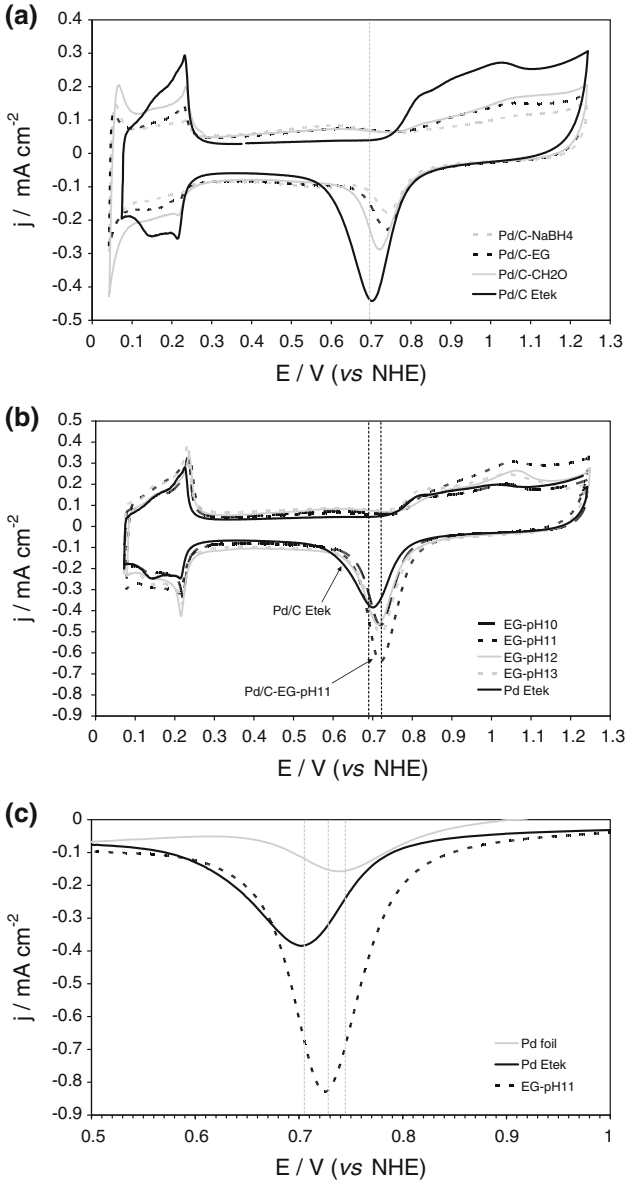

Fig. 5 Cyclic voltammograms of various Pd/C catalysts in N_2 saturated 0.5M H_2SO_4 at room temperature, scan rate 5 mV s^{-1}. **a** Full voltammogram showing the effect of reducing agent EG, $NaBH_4$ &CH_2O on home-made Pd/C with commercial Pd/C as bench mark. **b** Full voltammogram showing the effect of pH on home-made Pd/C with EG as reducing agent along with commercial Pd/C as bench mark. **c** a fragment of the cathodic voltammogram in the potential range 1–0.5 V of commercial Pd/C, Pd foil (Aldrich) and home-made Pd/C EGpH11

As previously discussed, shifts in the position of the palladium reduction peak were believed to be related to size of the palladium nanoparticles. All four catalysts prepared by EG reduction in basic conditions gave the palladium reduction peak at 0.72 V, ca. 20 mV lower than Pd/C–EG. This agreed with XRD observations, from which the particle size calculated was around 6 nm, smaller than the 11 nm of Pd/C–EG. The Pd/C–CH_2O catalyst, with

5 nm nanoparticles, very close to sizes of those four catalysts prepared in alkaline conditions, gave a palladium oxide reduction peak at the same potential, 0.72 mV. Cyclic voltammograms in N_2 saturated solution were also compared with that of a Pd foil electrode (Fig. 5c). Pd foil exhibited a palladium reduction peak at 0.74 V, providing this way further evidence of the dependence of the position of the palladium reduction peak with the particle size.

ECSA was higher for catalysts prepared by EG reduction in alkaline conditions compared to Pd/C–EG, as expected from their smaller particle sizes. Electrochemical surface areas corresponding to Pd/C–EG10, Pd/C–EG11, Pd/C–EG12 and Pd/C–EG13 were 12, 15, 11 and 15 $m^2\ g^{-1}$, respectively. The smallest ECSA was calculated for Pd/C–EG12, which had the largest particle size, 8 nm compared to 6 nm for the other three. The greatest active areas were obtained for catalysts prepared at pH 11 and 13. This, together with the catalyst morphology and the kinetic parameters obtained from the study of the ORR, led to the selection of pH11 for the synthesis of carbon-supported nanoparticles.

Carbon-supported palladium nanoparticles were also prepared on as-received Vulcan XC-72R using ethylene glycol as reducing agent at pH 11 (Pd/C–EG11-untr). Its ECSA was 15 $m^2\ g^{-1}$, the same value as for Pd/C–EG11, prepared on pre-treated carbon. Double layer charging current and the area of the oxide reduction peak were larger for the catalyst supported on pre-treated carbon due to the presence of functional groups on its surface [24] and the higher metal loading, respectively. The hydrogen sorption–desorption and the oxidation–reduction reactions of the Pd nanoparticles occurred at the same potentials for both catalysts. As concluded from XRD analyses, treatment under H_2 at 300 °C increased the size of Pd particles in every catalyst prepared. A decrease in the ECSA, which was a direct consequence of the particle size growth, was recorded for every treated catalyst (Table 1).

3.3 Oxygen reduction reaction

During LSV hysteresis appeared between the forward and backward potential sweeps. Currents in the anodic scan were larger than those in the prior cathodic scan at potentials above ca. 0.7 V. This behaviour was widely known for platinum electrodes and it was demonstrated to be due to the different oxide coverage of the electrode during both scans [41]. Studies have also shown the oxygen coverage of the Pd surface depends on the electrode potential and the electrode history [42]. Therefore, by analogy with platinum [43], the difference between both scans in a palladium electrode was attributed to the different oxide coverage of the metal surface. Since the aim of this work was to study the ORR on a palladium surface, not on palladium oxide, the anodic LSV was chosen because it was understood to be the one with the minimum oxide coverage. Figure 6 compares voltammograms in oxygen saturated electrolyte of Pd/C catalysts initially prepared using three different reducing agents. Onset potentials for Pd/C–$NaBH_4$, Pd/C–CH_2O and Pd/C–EG, were 0.86, 0.86 and 0.84 V, respectively (Table 2). All three onset potentials were at least 0.1 V lower than the Pt commercial catalysts, 0.96 V versus NHE.

Mass activity (MA) of Pd/C–$NaBH_4$, Pd/C–CH_2O and Pd/C–EG was compared at 0.75 V, where current densities were significant for all catalysts. The highest MA at 0.75 V was presented by Pd/C–EG, 7 A g^{-2} Pd (Table 2), which was close to the MA of Pd/C from Etek, 9 A g^{-2} Pd, but still only about 15% of the MA of Pt/C from Etek, 45 A g^{-2} Pt. The Pd/C–EG catalyst also presented the highest specific activity (SA) at 0.75 V, 118 μA cm^{-2} Pd. Interestingly, the SA was higher than for Pd/C and Pt/C from Etek, 56 and 83 μA cm^{-2} Pd, respectively. The fact that Pd/C–EG had higher MA and SA than Pd/C synthesised using CH_2O or $NaBH_4$, could be attributed to a better catalyst morphology (as shown in Fig. 1), a consequence of the use of this milder reducing agent. Similar behaviour was reported for palladium–cobalt catalysts by Zhang et al. [29].

Figure 7 shows LSVs for Pd/C catalysts prepared using EG as a reducing agent and controlling the pH of the system. In every case the onset potential increased by between 20 and 30 mV with respect to the catalyst prepared without pH control. Recorded onset potentials were 0.88, 0.89, 0.89 and 0.87 V for Pd/C–EG10, Pd/C–EG11, Pd/C–EG12 and Pd/C–EG13, respectively. Although, there were no significant differences in onset potentials between these four catalysts, highest onset potentials were for Pd/C–EG11 and Pd/C–EG12, 0.89 V. This was believed to be

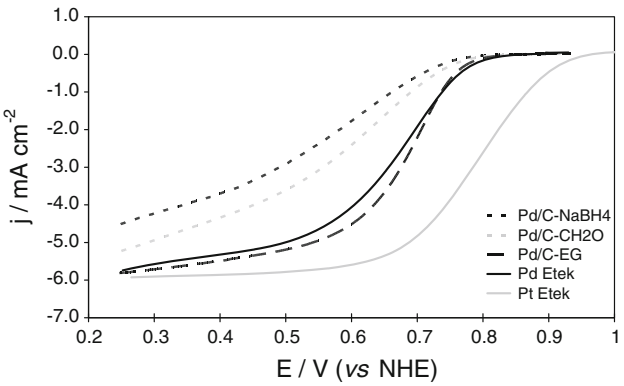

Fig. 6 Linear sweep voltammograms of Pt/C (Etek), Pd/C (Etek), Pd/C–EG, Pd/C–CH_2O and Pd/C–$NaBH_4$ catalysts. LSVs were recorded in O_2 saturated 0.5 M H_2SO_4 solution at room temperature, scan rate 1 mV s^{-1} and metal loading 86 μg cm^{-2}. LSVs are compared with those of the commercial Pd/C and Pt/C from Etek

Table 2 Tafel slope, transfer coefficient, exchange current density and onset potential for various carbon-supported Pd catalysts

Catalyst	Onset potential (V vs. NHE)	Tafel slope (mV dec^{-1})	Transfer coefficient	Exchange current density (A cm^{-2})	Mass activity at 0.75 V (A g^{-1} Pd)
Pd/C–EG	0.86	62	0.93	6.0×10^{-12}	7.2
Pd/C–EG-300	0.83	60	0.96	8.5×10^{-12}	2.9
Pd/C–CH_2O	0.86	62	0.93	2.2×10^{-12}	3.9
Pd/C–$NaBH_4$	0.84	62	0.94	2.7×10^{-12}	2.4
Pd/C–EG10	0.88	60	0.96	9.7×10^{-12}	16.4
Pd/C–EG11	0.89	59	0.98	7.7×10^{-12}	19.6
Pd/C–EG12	0.89	60	0.96	1.0×10^{-11}	15.7
Pd/C–EG13	0.87	62	0.93	8.6×10^{-12}	15.7
Pd/C-untr	0.89	59	0.98	1.0×10^{-11}	29.7
Pd/C-Etek	0.86	64	0.90	5.2×10^{-12}	8.8
Pt/C-Etek	0.96	64	0.91	1.4×10^{-10}	45.3
		128	0.45	6.1×10^{-8}	

due to the higher metal loading of these two catalysts, 34 and 29% weight, respectively. All mass activities at 0.75 V, were more than double that of the MA for Pd/C–EG, and in the range of 16–20 A g^{-2}: Pd/C–EG11, being the highest, 20 A g^{-2} Pd. This value was twice the MA of Pd/C from Etek, at 9 A g^{-2} Pd, and nearly thrice that of the MA of Pd/C–EG, but still was considerably lower than 45 A g^{-2} of Pt/C from Etek. Specific activities were all relatively similar to the SA of Pd/C–EG, 118 μA cm^{-2} Pd: 140, 127, 147 and 103 μA cm^{-2} Pd for Pd/C–EG10, Pd/C–EG11, Pd/C–EG12 and Pd/C–EG13, respectively.

Mass activities of Pd/C–EG11 and Pd/C-untr were also measured at 0.80 V in order to compare them with the available literature: values were 7.8 and 9.4 A g^{-1} for Pd/C–EG11 and Pd/C-untr, respectively. Mass activity for carbon-supported Pd nanoparticles have been reported in the same range, 8.4 A g^{-1} Pd at 0.8 V, by Wang et al., but not specific activity values were reported [44]. On the other hand, mass activities over one order of magnitude larger than these reported here, ca. 230 A g^{-1} at 0.80 V, have been reported by Shao et al. using a thinner catalysts layer, 10 μg cm^{-2}. The specific activity reported by the latter group was approximately one order of magnitude larger than these reported here, ca. 520 μA cm^{-2}, compare to 51 and 64 μA cm^{-2} at 0.8 V for Pd/C–EG11 and Pd/C-untr, respectively [8].

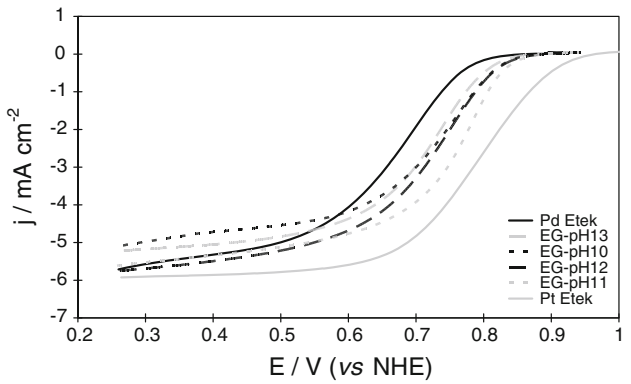

Fig. 7 Linear sweep voltammograms of Pt/C (Etek), Pd/C (Etek) Pd/C–EG10, Pd/C–EG11, Pd/C–EG12 and Pd/C–EG13 catalysts. LSVs were recorded in O_2 saturated 0.5 M H_2SO_4 solution at room temperature, scan rate 1 mV s^{-1} and metal loading 86 μg cm^{-2}

Palladium catalysts prepared by EG reduction in basic media presented similar specific activities and improved mass activities compared to the palladium catalyst prepared by EG reduction without pH control. This similarity in the specific activities would indicate that the morphology of the catalyst surface, for ORR, was similar for all five catalysts. The morphology of the catalyst surface obtained using EG as reducing agent was not affected by the pH of the reaction system. On the other hand, particles were smaller for catalysts prepared in alkaline conditions; this led to catalysts with higher surface areas and therefore higher mass activities.

Tafel analysis of data in the kinetically controlled region were taken from near-steady-state linear sweep voltammograms at scan rate 1 mV s^{-1}. Data was corrected for mass transport effects, using the correction parameter, $i \times i_L/(i_L - i)$ where i represents the current density at any potential and i_L the limiting current density [45]. Tafel plots, potential versus logarithm of current density, are shown in Fig. 8 Tafel plots were linear in the low current density region over ca. one order of magnitude of the current density. Figure 8a shows Tafel plots for Pd/C-Etek, Pd/C–EG, Pd/C–CH_2O and Pd/C–$NaBH_4$. Figure 8b shows Tafel plots for

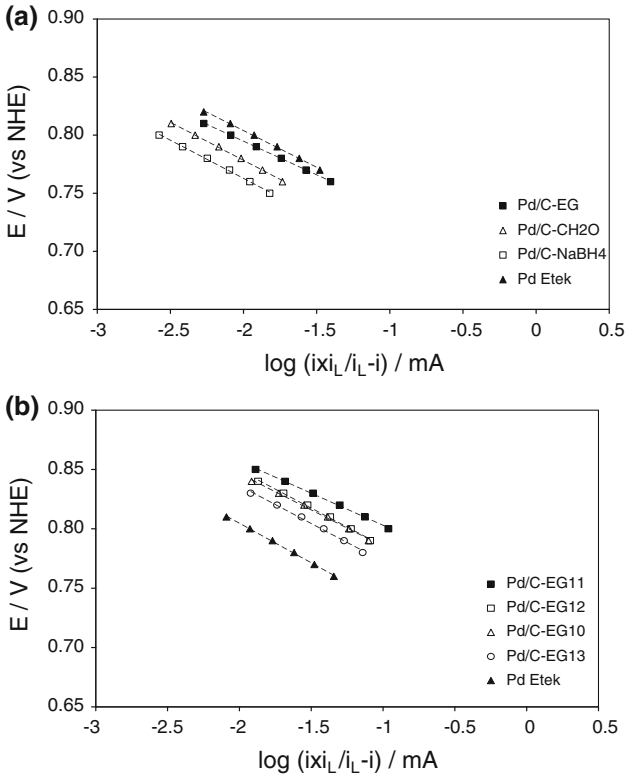

Fig. 8 Tafel plots for various Pd/C catalysts

Pd/C catalysts prepared by ethylene glycol reduction at different alkaline pH, Pd/C–EG10, Pd/C–EG11, Pd/C–EG12 and Pd/C–EG13. Plots were approximately parallel, all carbon-supported palladium catalysts exhibited Tafel slopes, b, ranging from 59 to 64 mV decade^{-1}. In the case of the Pt catalysts two Tafel slopes were observed. The slope in the low current density region was 64 mV decade^{-1} and the slope in the high current density region was 128 mV decade^{-1}.

Tafel slopes of ca. 60–70 mV decade^{-1} have been previously reported for Pd and Pd alloys in 0.5 M H_2SO_4 [29, 46–49]. It was reported that the mechanism of the ORR at a palladium electrode is the same that at a platinum electrode [43, 50] and that the low Tafel slope for a platinum electrode, 60 mV decade^{-1}, corresponds to a oxygen reduction taking place on a oxide-covered platinum electrode. Thus, it was concluded that all Tafel slopes reported for our palladium catalysts correspond to ORR on oxide-covered palladium electrodes.

Exchange current densities were obtained by extrapolating the Tafel line to the equilibrium potential. The equilibrium potential value used was 1.21 V after correcting the standard reduction potential for oxygen concentration, using the solubility value of O_2 in 0.5 M H_2SO_4, 1.02×10^{-3} M [51] and the Nernst equation. Exchange current densities, given in Table 2, were 6.0×10^{-12}, 2.2×10^{-12} and 2.7×10^{-12} A cm^{-2} for Pd/C–EG, Pd/C–CH_2O and Pd/C–$NaBH_4$, respectively. Exchange current densities for catalysts synthesized monitoring the pH were 9.7×10^{-12}, 7.7×10^{-12}, 1.0×10^{-11} and 8.6×10^{-12} A cm^{-2} for Pd/C–EG10, Pd/C–EG11, Pd/C–EG12 and Pd/C–EG13, respectively. These exchange current densities were close to the ones reported for palladium by Gnanamuthu et al. and by Tilak et al. [46, 50], 10^{-11} A cm^{-2}, but they were over an order of magnitude lower that the value reported by Savadogo et al. for palladium, 2.2×10^{-10} A cm^{-2} [48]. All palladium catalysts prepared using ethylene glycol, had an exchange current density close to 10^{-11} A cm^{-2}, which would mean that the morphology for the ORR was similar in all the five catalysts. The Pd/C–CH_2O and Pd/C–$NaBH_4$, gave exchange current densities closer to 10^{-12} A cm^{-2}. This would indicate that the morphology of a Pd/C catalyst was less favourable for the ORR when the reducing agent used in the synthesis was either formaldehyde or sodium borohydride.

ORR activity for catalyst further reduced in hydrogen at 300 °C, i.e. Pd/C–EG-300, was also studied. A decrease in the mass activity of Pd/C–EG-300 compared to Pd/C–EG, from 7 to 3 A g^{-1}, was observed at 0.75 V. This fall was believed to be due to the loss of catalyst surface area caused by particle growth during heat treatment. Exchange current density of Pd/C–EG-300, 8.5×10^{-12} A cm^{-2} Pd, and specific activity, 143 μA cm^{-2} Pd at 0.75 V, were not significantly different to the other Pd/C prepared by EG reduction. Since all heat treated catalysts suffered a loss of ECSA compared to the untreated catalyst, ORR activity studies for other treated catalysts were not carried out.

Activity towards the oxygen reduction reaction of Pd/C–EG11-untr was also evaluated. The Pd/C–EG11 and Pd/C–EG11-untr catalysts gave similar particle sizes, 6 and 7 nm, respectively calculated for XRD patterns, and similar ECSA, 15 m^2 g^{-1}, calculated from cyclic voltammograms in N_2 saturated electrolyte. Therefore it was not surprising that onset potentials and exchange current densities were also similar; 0.89 V and 1.0×10^{-11} A cm^{-2}, respectively, for both catalysts. However the current density at 0.75 V was higher for Pd/C–EG11-untr, which led to higher mass and specific activities, 30 A g^{-2} Pd and 201 μA cm^{-2} Pd, respectively. The slight increase in current density at 0.75 V together with the decrease in the amount of carbon lost, previously mentioned, and the simplicity of the synthesis, led to the selection of Pd/C–EG11-untr as the catalyst of choice for further investigations. Thus, pre-treatment of the carbon support with HNO_3 was no longer carried out for practical reasons.

3.4 Low temperature PEM fuel cell

The optimized carbon-supported palladium, Pd–EG11, prepared by reduction of the palladium precursor with

ethylene glycol on as-received Vulcan XC-72R, was tested as a cathode catalyst in a low temperature PEM fuel cell. Results are compared with those of a MEA with Pt/C and Pd/C from Etek in the cathode. Figure 9 shows cell polarization curves for the Pd–EG11, Pd/C-Etek and Pt/C-Etek MEAs at different operating temperatures. Onset potential, current densities at 0.5 V and peak power densities are given in Table 3.

A difference of approximately 200 mV in the open circuit potential (OCP) between Pd and Pt MEAs was observed in both oxygen and air polarization curves at 20 °C (Fig. 9a, b). The Pd/C based MEA gave an onset potential of 0.89 V versus NHE in the half cell characterization, 70 mV lower than Pt/C from Etek. The increased difference in the OCP between Pd and Pt when tested in the PEM fuel cell can be explained by the H_2 cross-over through the electrolyte membrane. The impact of this cross-over would have been higher in Pd due to its lower exchange current density for the ORR. The observed OCP in a fuel cell is always lower than the estimated value from the thermodynamics, E_{rev}, due to the effect of cross-over and other phenomena like carbon corrosion [52]. The crossover would also be the reason why the activation region could hardly be seen in polarization curves of the Pd MEAs. The overpotential caused by the crossover at low current densities masked the kinetic region of the polarization curve. A near constant difference of 110 mV existed in the ohmic region between Pd/C–EG 11 and Pt MEAs. While Pd/C (Etek) exhibited smaller average particles size and therefore showed higher current in the kinetic region in comparison to Pd/C–EG 11 at 20 °C, its I–V slope was worse than Pd/C–EG 11. The difference in the slope could not have been caused by membrane effects (IR) or electrode effects (mass transport) as both MEAs used identical materials and catalyst loading. The difference in the slope must have arisen from a difference in Tafel slope in the high current region between the two catalysts. Similar result was obtained in half cell tests between Pd/C–EG and Pd/C-Etek (Fig. 6).

Peak power densities at 20 °C with Pd/C–EG 11 in the cathode were 183 and 520 mW cm^{-2} with air and oxygen, respectively. In comparison, Pd/C-Etek showed similar peak power density of 174 and 558 mW cm^{-2} with air and oxygen, respectively.

When the temperature was increased to 40 °C a reduced difference between Pt and Pd MEA performance was observed (Fig. 9c, d). The potential difference obtained between the two MEAs in the Ohmic region was 60 mV. This could be explained by the higher activation energy of oxygen reduction reaction on Pd/C, ca. 90 kJ mol^{-1} [53], compared to that on Pt, ca. 26 kJ mol^{-1} [54]. The peak power density at 40 °C with Pd/C–EG 11 in the cathode

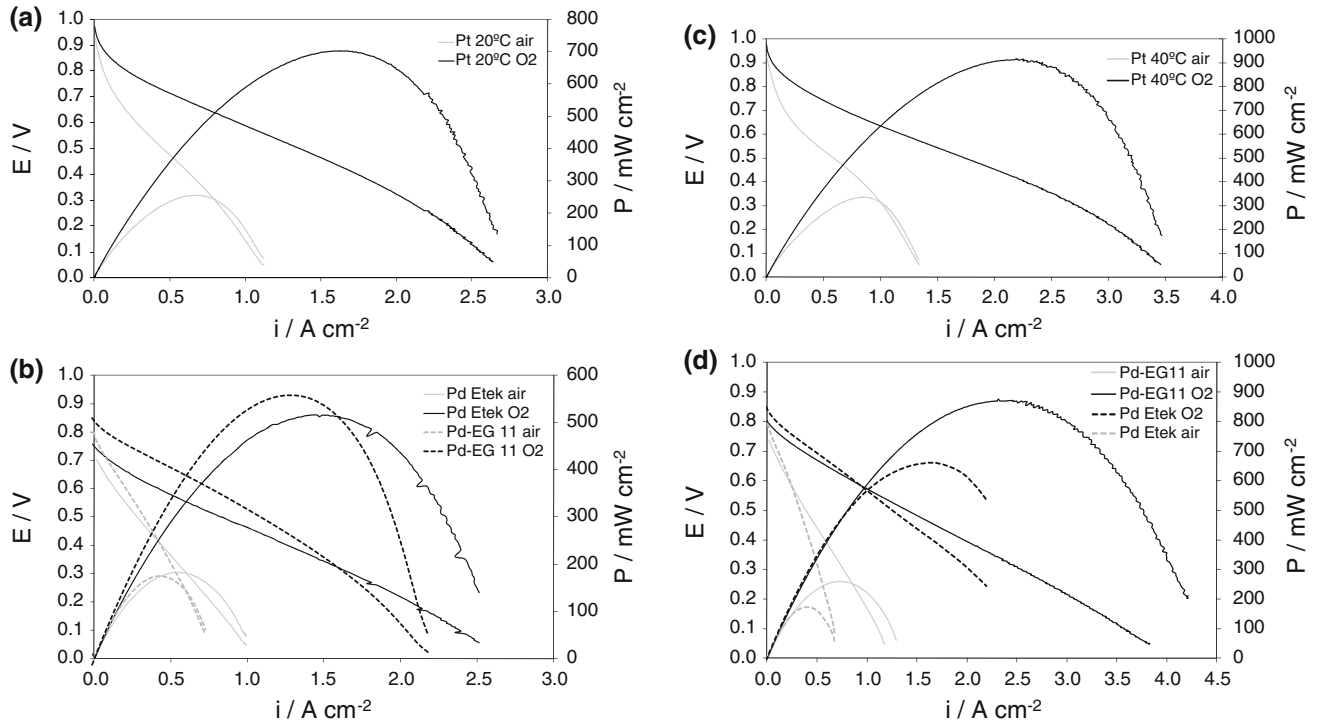

Fig. 9 Polarization curves at scan rate 5 mV $^{s-1}$ and power density of low temperature PEM fuel cell using H_2 fed anode and air or O_2 fed cathode; gases were fed at atmospheric pressure. Data was collected with Nafion® 112 membrane, anode catalyst loading of 0.2 mg cm^{-2} of Pt from Etek and cathode loading of 0.6 mg cm^{-2} of Pt/C-Etek, Pd/C-Etek or home-made Pd/C Pd–EG11. **a** Pt/C-Etek at 20°C, **b** Pd/C-Etek and Pd–EG11at 20°C, **c** Pt/C-Etek 40°C and **d** Pd/C-Etek and Pd–EG11at 40°C

Table 3 Onset potential, current density at 0.5 V and peak power density measured of a low temperature PEM fuel cell at different temperatures operating on H_2 and air or O_2 with different electrocatalysts in the cathode

Cathode catalyst	Temperature (°C)	Cathode feeding	Onset potential (V)	Current density at 0.5 V (A cm^{-2})	Peak power density (mW cm^{-2})
Pd–EG11	20	Air	0.71	0.27	183
Pd–EG11	20	O_2	0.75	0.82	520
Pd–EG11	40	Air	0.74	0.38	259
Pd–EG11	40	O_2	0.80	1.38	872
Pt/C-Etek	20	Air	0.93	0.45	255
Pt/C-Etek	20	O_2	0.95	1.26	702
Pt/C-Etek	40	Air	0.93	0.59	335
Pt/C-Etek	40	O_2	0.97	1.74	914

was 259 and 872 mW cm^{-2} with air and oxygen, respectively. This was significantly higher than that of Pd/C-Etek which achieved at 40 °C power density of 170 and 661 mW cm^{-22} with air and oxygen, respectively.

In the literature activities for Pt and Pd as cathode materials were reported lower than our measurements. For instance Fiçicilar et al. [55] reported activities of carbon-supported Pd and Pt nanometric particles, at 0.5 V current densities of ca. 0.1 and 0.35 A cm^{-2}, and cell potentials at 0.5 A cm^{-2} ca. 0.24 and 0.35 V, respectively. This performance was in a PEM operating on pure H_2 and O_2 at 70 °C with a metal loading of 0.4 mg cm^{-2} in both anode and cathode. Our fuel cell gave current densities of 0.82 and 1.26 A cm^{-2} at 0.5 V, and cell potentials at 0.5 A cm^{-2} ca. 0.58 and 0.69 V for Pd and Pt cathodes, respectively. The potential difference in the ohmic region between Pd/C and Pt/C was in both cases 110 mV. Considerably lower activity for Pd on Vulcan was reported by Moreira and Ficicilar et al. [18, 55], with current density values of ca. 0.04 A cm^{-2} at 0.5 V. This performance was in a PEM operating on pure H_2 and O_2 at room temperature with a metal loading of 0.4 mg cm^{-2} in the anode and 1 mg cm^{-2} in the cathode.

3.5 Evaluation of higher loading palladium electrodes

Since palladium is approximately four times cheaper than platinum the use of larger amounts of Pd in the cell cathode is appropriate to see if there is an economic advantages. In this section a MEA with cathode loading 1.0 mg cm^{-2} of Pd are compared with MEAs with cathode loadings of 0.6 mg cm^{-2} of Pd or Pt.

Figure 10a, b compare polarization curves of palladium MEAs with different cathode metal loadings at 20 and 40 °C, respectively. The increase of the cathode metal loading from 0.6 to 1.0 mg cm^{-2} produced a large increase in current density in the kinetic region (low current densities). At 20 °C operating with air the open circuit voltage increased by 0.14 V, from ca. 0.71 to 0.85 V. Operating with oxygen at 20 °C the OCP increase was also 0.14 V. When the operating temperature was 40 °C a similar effect was observed in the cell OCP. Cathode metal loading 1.0 mg cm^{-2} exhibited an OCP 0.15 and 0.13 V higher than loading 0.6 mg cm^{-2}, with air and oxygen, respectively. This is in accord with the previous analysis of the crossover impact on Pd, increasing the loading will increase the ECSA and i0 accordingly leading to a smaller impact of crossover.

On the other hand, in the high current density region the MEA with lower cathode metal loading exhibited higher cell potentials. This phenomenon was attributed to mass transport effects. Differences in the slopes between polarization curves of the two MEAs (Fig. 10) indicated that the MEA with larger cathode loading was suffering from mass transport problems, since membrane and operating conditions were the same for both MEAs. This also can be seen from the difference between oxygen and air operation for a given current density is significantly higher in the double loading than the single loading MEA.

4 Conclusions

Palladium nanoparticles supported on pre-treated Vulcan XC-72R were synthesized without pH control using an impregnation method followed by a reduction with three different reducing agents: ethylene glycol, formaldehyde and sodium borohydride. Formaldehyde reduction yielded the smallest Pd nanoparticles, around 5 nm, however, ethylene glycol produced the catalyst with higher mass and specific activities, 7 A g^{-1} Pd and 118 μA cm^{-2} Pd, respectively. It was found that reduction of $(NH_4)_2PdCl_4$ lead to smaller particles, around 6 nm, when carried out at basic pH, between 10 and 13 pH units. The pH of the reaction system caused an increase in the dispersion on the carbon surface and a decrease in the size of palladium

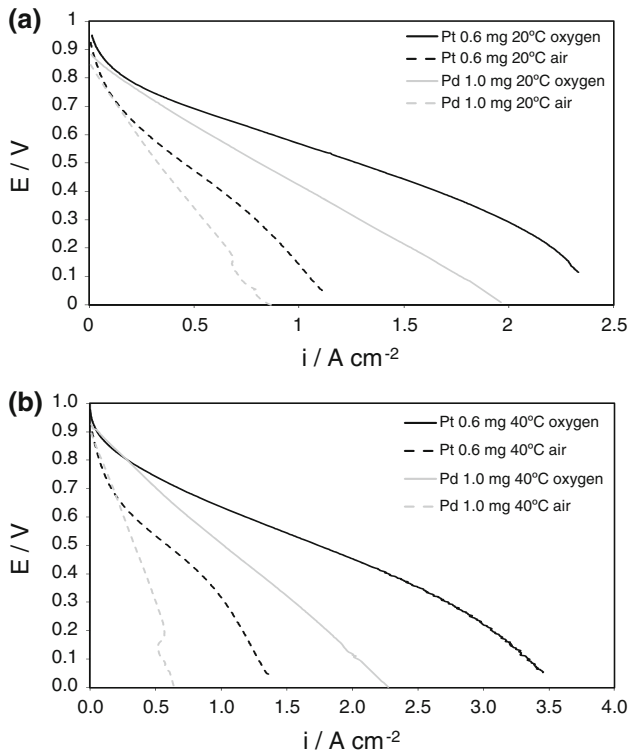

Fig. 10 Comparison of polarization curves of a low temperature PEMFC with cathode loadings 1 mg cm^{-2} of Pd/C–EG11 and 0.6 mg cm^{-2} Pt/C-Etek. **a** at 20°C and **b** at 40°C

nanoparticles. The Exchange current density of ORR on Pd/C catalysts prepared by EG reduction, was close to 10^{-11} A cm^{-2} Pd.

All carbon-supported palladium catalysts exhibited only one Tafel slope, in the low current density region, with values ranging from 59 to 64 mV $decade^{-1}$. In the high current density region a constantly changing Tafel slope was observed. This change in Tafel slope was believed to be due to the change of the oxygen coverage of the catalyst surface with the potential.

Heat treatment in H_2 at 300 °C caused particle growth on all carbon-supported palladium nanocatalysts and therefore a decrease in their mass activity.

Carbon supported Pd nanoparticles prepared by reduction by ethylene glycol exhibited relatively good performance in low temperature hydrogen PEMFCs. They showed good potential to close the gap with Pt/C catalyst. Peak power densities obtained from the Pd–EG11 MEA with O_2 and air (atm) were 872 and 259 mW cm^{-2} at 40 °C, which compares closely with those obtained with the Pt/C-Etek MEA; 914 and 335 mW cm^{-2} at 40 °C with O_2 and air (atm), respectively.

Acknowledgements The work described in this paper was supported by the EPSRC SUPERGEN fuel cell consortium award.

References

1. Gasteiger HA, Kocha SS, Sompalli B et al (2005) Appl Catal B 56:9
2. Xiong L, Manthiram A (2005) Electrochim Acta 50:2323
3. Xiong L, Kannan AM, Manthiram A (2002) Electrochem Commun 4:898
4. Salgado JRC, Antolini E, Gonzalez ER (2004) J Electrochem Soc 151:A2143
5. Paulus UA, Wokaun A, Scherer GG et al (2002) J Phys Chem B 106:4181
6. Ioroi T, Yasuda K (2005) J Electrochem Soc 152:A1917
7. Fernández JL, Raghuveer V, Manthiram A et al (2005) J Am Chem Soc 127:13100
8. Shao M-H, Sasaki K, Adzic RR (2006) J Am Chem Soc 128:3526
9. Wang X, Kariuki N, Vaughey JT et al (2008) J Electrochem Soc 155:B602
10. Mustain WE, Kepler K, Prakash J (2006) Electrochem Commun 8:406
11. Papageorgopoulos DC, Keijzer M, Veldhuis JBJ et al (2002) J Electrochem Soc 149:A1400
12. Machida K, Enyo M (1987) J Electrochem Soc 134:1472
13. Lewis FA (1982) Platin Met Rev 26:20
14. Damjanovic A, Brusic V (1967) Electrochim Acta 12:1171
15. Chaston JC, Sercombe EJ (1961) Platin Met Rev 5:122–125
16. Pope D, Smith WL, Eastlake MJ et al (1971) J Catal 22:72
17. Bond GC (1975) Platin Met Rev 19:126
18. Moreira J, del Angel P, Ocampo AL et al (2004) Int J Hydrog Energy 29:915
19. Fernández JL, Walsh DA, Bard AJ (2004) J Am Chem Soc 127:357
20. Salgado JRC, Antolini E, Gonzalez ER (2004) J Phys Chem B 108:17767
21. Chan K-Y, Ding J, Ren J et al (2004) J Mater Chem 14:505
22. Larcher D, Patrice R (2000) J Solid State Chem 154:405
23. Li H, Sun G, Gao Y et al (2007) J Phys Chem C 111:15192
24. Guha A, Lu W, Zawodzinski TA Jr et al (2007) Carbon 45:1506
25. Mallát T, Polyánszky É, Petró J (1976) J Catal 44:345
26. Breiter MW (1977) J Electroanal Chem 81:275
27. Lee K, Savadogo O, Ishihara A et al (2006) J Electrochem Soc 153:A20
28. Suo Y, Zhuang L, Lu J (2007) Angew Chem Int Ed 46:2862
29. Zhang L, Lee K, Zhang J (2007) Electrochim Acta 52:7964
30. Canton P, Meneghini C, Riello P et al (2001) J Phys Chem B 105:8088
31. Jiang L, Hsu A, Chu D et al (2009) J Electrochem Soc 156:B643
32. Burke LD, Buckley DT (1996) J Electrochem Soc 143:845
33. Burke LD, Casey JK (1993) J Electrochem Soc 140:1284
34. Rand DAJ, Woods R (1972) J Electroanal Chem 35:209
35. Solla-GulloÌon J, Montiel V, Aldaz A, Clavilier J (2003) J Electrochem Soc 150:E104–E109
36. Zeng J, Lee JY, Zhou W (2006) Appl Catal A 308:99
37. Mukerjee S, McBreen J (1998) J Electroanal Chem 448:163
38. Li H, Sun G, Jiang Q et al (2007) Electrochem Commun 9:1410
39. Grigoriev SA, Millet P, Fateev VN (2008) J Power Sour 177:281
40. Luo C, Zhang Y, Wang Y (2005) J Mol Catal A Chem 229:7
41. Damjanovic A, Brusic V (1967) Electrochim Acta 12:615
42. Sleightholme AES (2007) Electrochemical studies of fuel cell catalysts. PhD thesis, Imperial College, London
43. Damjanovic A (1967) J Phys Chem 71:2741
44. Wang X, Kariuki N, Myers D et al (2006) DOE hydrogen program. Annual Progress Report FY 2006:791
45. Parthasarathy A, Martin CR, Srinivasan S (1991) J Electrochem Soc 138:916
46. Gnanamuthu DS, Petrocelli JV (1967) J Electrochem Soc 114:1036

47. Mustain WE, Kepler K, Prakash J (2006) Electrochimica Acta 52:2102–21028
48. Savadogo O, Lee K, Oishi K et al (2004) Electrochem Commun 6:105
49. Hoare JP (1965) J Electrochem Soc 112:1129
50. Tilak BV, Tari K, Hoover CL (1988) J Electrochem Soc 135: 1386
51. Gubbins KE, Walker RDJ (1965) J Electrochem Soc 112:469
52. Scott K, Mamlouk M (2009) Int J Hydrog Energy 34:9195
53. Mustain WE, Prakash J (2007) J Power Sour 170:28
54. Paulus UA, Schmidt TJ, Gasteiger HA et al (2001) J Electroanal Chem 495:134
55. Ficicilar B, Bayrakceken A, Eroglu I (2009) J Power Sour 193:17